Advances in Geo-Energy Research

Vol. 17, No. 1, p. 82-90, 2025

Original article

Borehole full-waveform inversion of monopole logging in slow formations: Insights for shear-wave velocity profiling

Song Xu[1,2]*, Ying Liu[1,2], Zhihui Zou[1,2], Yukai Liu[3]

[1]*Key Laboratory of Submarine Geosciences and Prospecting Techniques MOE, College of Marine Geosciences, Ocean University of China, Qingdao 266100, P. R. China*

[2]*Laboratory for Marine Mineral Resources, Qingdao Marine Science and Technology Center, Qingdao 266237, P. R. China*

[3]*Department of Mechanical of Engineering, Eindhoven University of Technology, Eindhoven 5600MB, Netherlands*

Keywords:
Shear-velocity imaging
slow formation
borehole full-waveform inversion
monopole logging

Cited as:
Xu, S., Liu, Y., Zou, Z., Liu, Y. Borehole full-waveform inversion of monopole logging in slow formations: Insights for shear-wave velocity profiling. Advances in Geo-Energy Research, 2025, 17(1): 82-90. https://doi.org/10.46690/ager.2025.07.07

Abstract:
Slow formations, characterized by shear-wave velocities lower than those of the borehole fluid, present significant challenges for shear-wave velocity estimation using monopole acoustic logging, primarily due to the absence of critically refracted shear waves. To address this limitation, a borehole full-waveform inversion framework is proposed in this paper, which employs low-frequency monopole excitation to exploit the sensitivity of Stoneley waves to shear velocity. The elastic wave equation is reformulated in cylindrical coordinates as a recurrent neural network structure within a deep learning framework, allowing automatic differentiation for efficient gradient computation without adjoint-state methods. Numerical experiments reveal that while high-frequency monopole data can accurately recover compressional-wave velocities, they fail to resolve shear-wave velocities due to weak Stoneley energy in the high-frequency data. In contrast, strong low-frequency Stoneley waves enable robust and reliable shear-wave inversion. An inversion workflow is further proposed, in which an initial shear-wave velocity model is derived by applying a velocity ratio to the inverted compressional-wave model and subsequently refined through inversion of low-frequency monopole data. The proposed approach yields high-accuracy shear velocity profiles in the near-wellbore region and remains effective under complex geological conditions, including small-scale anomalies and ultra-slow formations. These results highlight the critical role of Stoneley waves in monopole-based inversion and offer a practical solution for estimating the shear-wave velocities of slow and unconsolidated formations.

1. Introduction

Shear-wave (S-wave) velocity is a key parameter for characterizing the mechanical properties of rocks, such as the Young's modulus, Poisson's ratio, and shear modulus (Mavko et al., 2020; Berg et al., 2021; Li et al., 2022; Wang et al., 2023b; Xu, 2024). Thus, it plays a critical role in drilling optimization, hydraulic fracturing design and borehole stability analysis (Zhang et al., 2009; Fan et al., 2025). Furthermore, S-wave velocity is minimally influenced by pore fluids and, in combination with compressional-wave velocity, contributes to identifying fluid distribution and characterizing reservoir properties. In slow formations where the S-wave velocity is lower than the velocity of the borehole fluid, critically refracted shear waves fail to form, making conventional logging techniques ineffective for estimating shear velocity (Tang and Cheng, 2004). To address the challenge of estimating S-wave velocity in slow formations, dipole acoustic logging was developed by Kurkjian and Chang (1986), where the propagation velocity

*Corresponding author.
E-mail address: xusongupc@sina.com (S. Xu); liouying@ouc.edu.cn (Y. Liu); zouzhihui@ouc.edu.cn (Z. Zou); Y.liu3@tue.nl (Y. Liu).

Received May 26, 2025; revised June 19, 2025; accepted July 5, 2025; available online July 10, 2025.

Yandy Scientific Press

of flexural waves near the low-frequency cutoff is typically used as an approximation of the formation's S-wave velocity. In cases where dipole measurements are unavailable, Stoneley waves can also be employed to indirectly infer S-wave velocity (Stevens and Day, 1986), as they exhibit a certain degree of sensitivity to the shear properties of the formation. In recent years, with the advancement of data-driven techniques, machine learning has been increasingly applied to S-wave velocity prediction (Wang et al., 2020; Ebrahimi et al., 2022; Rajabi et al., 2023), further extending the capabilities and applicability of conventional logging methods.

Several methods have been proposed for S-wave velocity profiling around boreholes, including joint inversion using Stoneley and flexural waves (Sinha et al., 2005), the introduction of constraints to address the nonuniqueness issue (Tang and Patterson, 2010), and the utilization of second-order flexural modes to enhance sensitivity (Li et al., 2023). However, first, these approaches commonly assume an exponential radial decay of shear velocity, which may not reflect the actual geological conditions (Wang and Zhang, 2018; Li et al., 2024). Second, most rely on point-based dispersion curve fitting, limiting axial resolution and reducing the effectiveness of full wavefield for high-resolution S-wave imaging. Third, borehole tomography methods (Hornby, 1993; Zeroug et al., 2006; Xu et al., 2024; Xu and Zou, 2025) fail to utilize refracted wave information within the formation, making them ineffective for S-wave velocity estimation in slow formations.

Recently, Borehole Full-Waveform Inversion (BFWI) has shown great potential for high-resolution velocity imaging by leveraging the full wavefield information in both time and space (Chen et al., 2023; Tang et al., 2023; Fang et al., 2024). Zhang et al. (2025) investigated S-wave inversion in slow formations using monopole BFWI and showed that, even in the absence of refracted S-waves, Stoneley waves can effectively be utilized for imaging shear velocity in layered, metamorphic and ultra-slow formations. While effective, this approach is constrained by the use of traditional adjoint-state gradient computation and the need for manually constructed initial models, reducing the flexibility and hindering scalability in practical scenarios.

To address the above limitations, a BFWI framework is presented in this paper, that integrates Automatic Differentiation (AD) with a Recurrent Neural Network (RNN) representation of the elastic wave equation in cylindrical coordinates. This approach fundamentally differs from the adjoint-state method in that it embeds both forward modeling and gradient computation within a unified deep learning structure, eliminating the need for explicit adjoint derivation and allowing for seamless gradient backpropagation through time. As a result, the inversion process becomes more flexible, easier to implement, and potentially more efficient in handling complex geometries and material contrasts. In addition, a practical strategy is introduced for constructing the initial S-wave model by scaling a high-resolution compressional-wave (P-wave) velocity model, derived from high-frequency monopole data, using a constant P-to-S wave velocity (V_P/V_S) ratio. S-wave velocity is then recovered through low-frequency monopole inversion by leveraging the sensitivity of Stoneley waves. Numerical experiments demonstrate the robustness and accuracy of the proposed method in both typical slow formations and more complex settings, including ultra-slow formations and velocity anomaly zones. This study offers an efficient and broadly applicable solution for S-wave velocity estimation in slow formations, extending the utility of BFWI in challenging borehole environments.

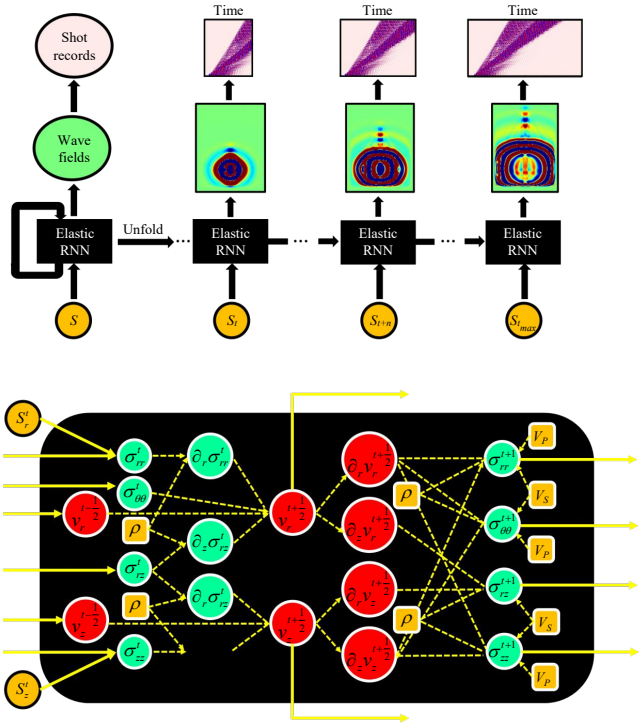

Fig. 1. Propagation of the particle velocity field formulated as a RNN, along with the architecture of each RNN cell.

2. Theory and method

BFWI is an advanced technique for reconstructing the elastic parameters (e.g., P-wave and S-wave velocities) of formations surrounding the borehole by minimizing the misfit between observed and simulated full waveform data. In full waveform inversion, the objective function E is typically defined as the squared L2 norm of the difference between synthetic and observed data, such as:

$$E(\mathbf{m}) = \frac{1}{2}\left\| w^{syn} - w^{obs} \right\|_2^2 \tag{1}$$

where $\mathbf{m} = (V_P, V_S)$ represents the model parameters; w^{obs} and w^{syn} are the observed and simulated waveforms, respectively.

To overcome the complexity of traditional adjoint-state gradient derivations, this study adopts an AD-based BFWI framework, AD-BFWI, which embeds the elastic wave equation into a RNN, treating the subsurface model $\mathbf{m}$ as trainable parameters (Wang et al., 2023a). This enables full-waveform inversion to be implemented within modern deep learning frameworks using automatic differentiation, avoiding manual derivation of adjoint equations and improving flexibility (Sun et al., 2020; Du et al., 2024). Fig. 1 illustrates the implementation of the elastic wave equation in cylindrical coordinates using a RNN.

The model decomposes wavefield propagation into a time-recursive structure, where particle velocities (radial and axial components) and stress components are updated step-by-step in a timely manner to simulate dynamic wavefield evolution. At its core, this approach transforms Partial Differential Equations (PDEs) into sequential RNN computational units. Spatial derivatives are approximated using finite-difference schemes, and wave propagation is achieved through the alternating update of stress and velocity fields. This design embeds physical laws directly into the deep learning framework, enabling forward modeling that is inherently compatible with automatic differentiation. It combines explicit physical constraints with end-to-end differentiability, providing a robust foundation for automatic gradient computation and multiparameter inversion. The optimization objective is defined as:

$$\arg_{\mathbf{m}} \min \left\{ E\left(\mathrm{WaveRNN}(\mathbf{m}, s, \mathbf{x}_r), w^{\mathrm{obs}}(s, \mathbf{x}_r)\right) + \lambda R(\mathbf{m}) \right\} \tag{2}$$

where WaveRNN represents the forward simulation operator that computes synthetic waveforms given the model $\mathbf{m}$, the source function s, and receiver positions $\mathbf{x}_r$; $w^{\mathrm{obs}}(s, \mathbf{x}_r)$ denotes the observed waveforms corresponding to the same acquisition configuration; λ denotes the regularization weight, and $R(\mathbf{m})$ is the total variation regularization term (Engl et al., 1996) used to stabilize the inversion. AD calculates the gradient via the chain rule by recording intermediate variables during forward propagation and applying backpropagation from the output to the input layers. This process yields the gradient of the objective function with respect to the model parameters as follows:

$$\mathbf{m}_{k+1} = \mathbf{m}_k - \alpha \nabla E(\mathbf{m}_k), \quad \nabla E(\mathbf{m}_k) = \mathrm{back}(E) \tag{3}$$

where α is the learning rate, and k denotes the iteration index. The gradient $\nabla E(\mathbf{m}_k)$ is automatically computed without requiring the manual derivation of adjoint-state equations. The term back denotes the backward algorithm, a widely used method in deep learning that efficiently computes gradients by applying the chain rule to the computational graph constructed during forward modeling. Compared to traditional full waveform inversion, the AD-based approach avoids manual derivation of the adjoint-state equations and offers greater flexibility and scalability for multi-parameter inversion.

3. Numerical results

3.1 Radially layered model

The first test model is a classical radially layered formation. The borehole has a radius of 10 cm and is filled with water, with a P-wave velocity of 1,500 m/s and a density of 1,000 kg/m^3. The surrounding formation is defined as a slow formation. The P-wave velocities of the inner, middle and outer layers are 2,000 m/s, 2,300 m/s and 2,500 m/s, respectively, and the corresponding S-wave velocities are 1,100 m/s, 1,200 m/s and 1,300 m/s. The formation rock density is uniformly set to 2,000 kg/m^3. The sources and receivers are uniformly arranged along the borehole axis with a spacing of 0.15 m. For each source excitation, all receivers are triggered simultaneously to record the wavefield data. According to typical monopole logging configurations, the source is modeled as a Kelly-type monopole source with central frequencies of 10 kHz and 2 kHz. The initial velocity model is constructed by applying a Gaussian filter with a standard deviation of 15 to the true velocity model.

Fig. 2 presents the BFWI results of P-wave (Figs. 2(a), 2(c)) and S-wave (Figs. 2(b), 2(d)) velocity models at different iteration steps under monopole excitation with central frequencies of 10 kHz and 2 kHz. Under the 10 kHz high-frequency monopole excitation, the P-wave velocity is well recovered (Fig. 2(a)), accurately delineating the layer interfaces and internal structures, especially with high resolution at the boundaries. However, the S-wave inversion result is significantly poorer (Fig. 2(b)), with only vague structural outlines near the interfaces and large deviations from the true S-wave velocities within the layers. This indicates that at high frequencies, the monopole source is much more sensitive to P-waves than to S-waves. This observation aligns with the theoretical expectations: in slow formations where the S-wave velocity is lower than the borehole fluid velocity, critically refracted shear waves cannot be excited, resulting in a lack of usable S-wave information for inversion. In contrast, under low-frequency excitation at 2 kHz (Figs. 2(c) and 2(d)), the inversion of S-wave velocity is significantly improved. The reconstructed model (Fig. 2(d)) accurately captures both the layer boundaries and intra-layer variations, indicating the enhanced sensitivity of low-frequency monopole wavefields to S-wave information. This improvement is primarily attributed to the strong presence of Stoneley waves at low frequencies. Stoneley waves are capable of propagating through slow formations and carry substantial S-wave content, thereby enhancing the resolution of shear velocity imaging. Additionally, although some perturbations are observed near layer interfaces in the P-wave inversion result (Fig. 2(c)), the overall velocity structure is still well recovered, suggesting that low-frequency data also retain useful P-wave information. In summary, high-frequency monopole logging (10 kHz) is more effective for extracting P-wave velocity information, whereas low-frequency logging (2 kHz) proves advantageous for retrieving S-wave velocity, particularly in slow formations where the S-wave velocity is lower than that of the borehole fluid. In such cases, low-frequency Stoneley waves play a key role in enabling successful S-wave inversion. Notably, similar trends were observed in surface-wave FWI using high-speed railway seismic data, where S-wave velocity inversion outperformed P-wave velocity inversion, which indirectly supports the validity of the conclusions drawn from borehole acoustic logging (Wang et al., 2025). The acoustic field characteristics underlying these observations are illustrated in Fig. 3.

In the time-domain waveforms acquired under 10 kHz monopole excitation (Fig. 3(a)), the initial arrivals are dominated by high-amplitude signals corresponding to borehole fluid waves. As the offset increases, the arrivals transition into refracted P-waves from different formation layers. This behavior forms the basis for P-wave velocity inversion using high-frequency full waveform inversion. Notably, the amplitude of Stoneley waves at this frequency is extremely weak, indicating that their contribution to inversion is negligible. Given that

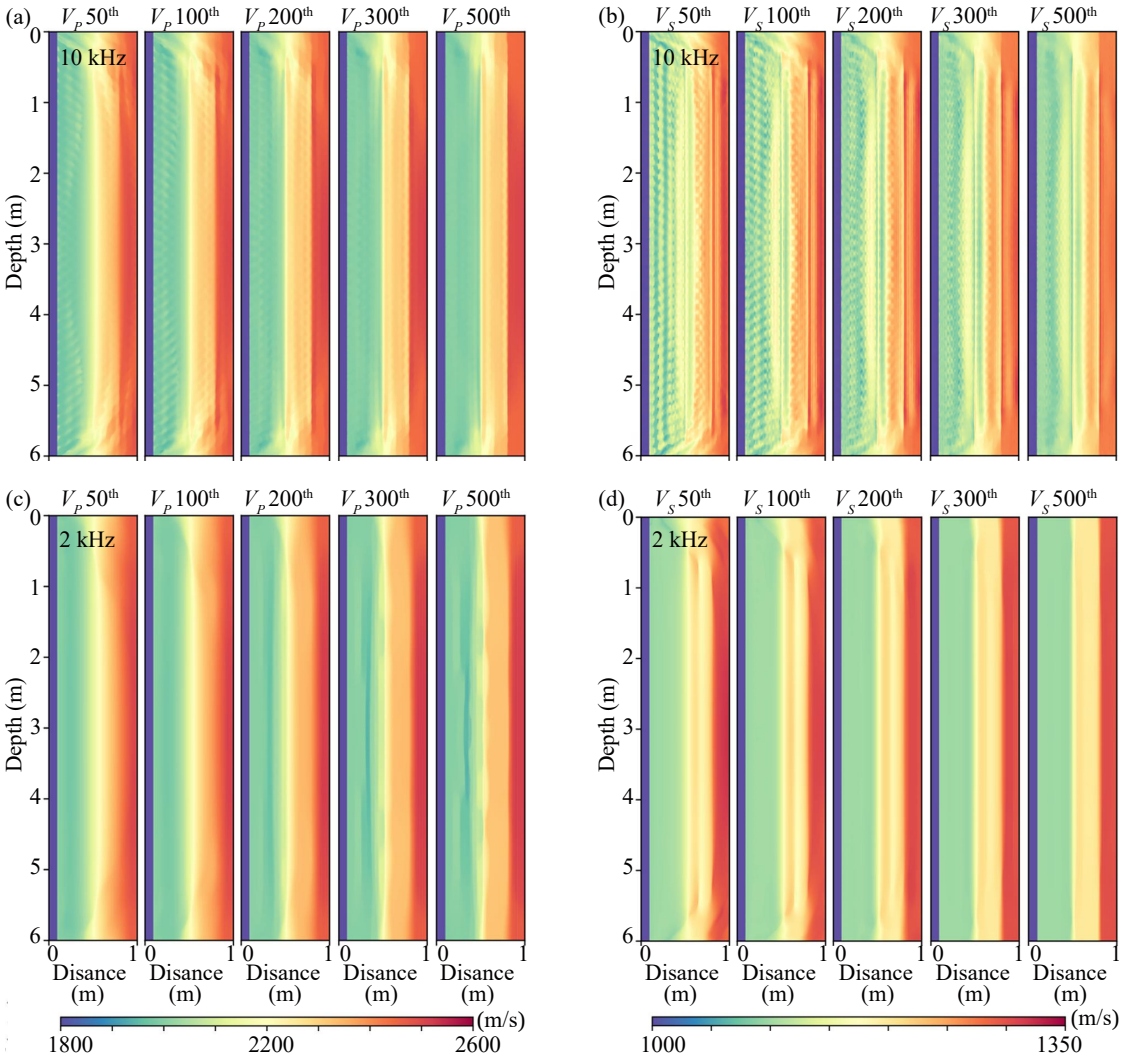

Fig. 2. Inversion results for P- and S-wave velocities under monopole excitation. (a) P-wave at 10 kHz; (b) S-wave at 10 kHz; (c) P-wave at 2 kHz; and (d) S-wave at 2 kHz.

Stoneley waves are sensitive to S-wave properties, this agrees with the poor S-wave recovery from high-frequency monopole data (Fig. 2).

In contrast, at 2 kHz, the Stoneley wave exhibits dominant amplitude, confirming that it is primarily excited at low frequencies. In addition, the waveform contains identifiable refracted P-waves, suggesting that low-frequency monopole excitation can still provide sensitivity to P-wave structures (see Fig. 2(c)). The normalized absolute difference between the true and initial models is plotted in Fig. 3(b). At 10 kHz, the largest discrepancies correspond to regions dominated by P-wave propagation. In contrast, the 2 kHz case exhibits stronger differences associated with Stoneley waves, while notable deviations also appear in zones influenced by P-wave energy. These results confirm that high-frequency data are more suitable for resolving P-wave velocities, whereas low-frequency measurements offer improved sensitivity to S-wave velocities, with some complementary value for P-wave imaging.

Wavefield snapshots at selected time steps are presented in Fig. 3(c) for high and low frequencies. Initially, the direct wave through the borehole fluid arrives first, followed by formation-reflected and refracted waves. Interface reflections, although weak, are also observable and represent valuable components of BFWI, as they help improve imaging resolution. At 2.8 ms, Stoneley waves are observed to radiate energy continuously into the formation, generating leaky waves and significantly attenuating their amplitude at far offsets. Consequently, reliable Stoneley wave signals are hardly detectable at large offsets under high-frequency excitation. On the other hand, low-frequency (2 kHz) wavefields exhibit longer wavelengths, reducing interface reflectivity. Thus, even though P-wave refractions are detectable, the dominant energy resides in the Stoneley wave, which accounts for the reduced accuracy in P-wave velocity recovery at low frequencies. However, the strong Stoneley wave presence enhances sensitivity to S-wave structures. Besides, the longer wavelength enables sufficient illumination of the entire formation thickness, making low-

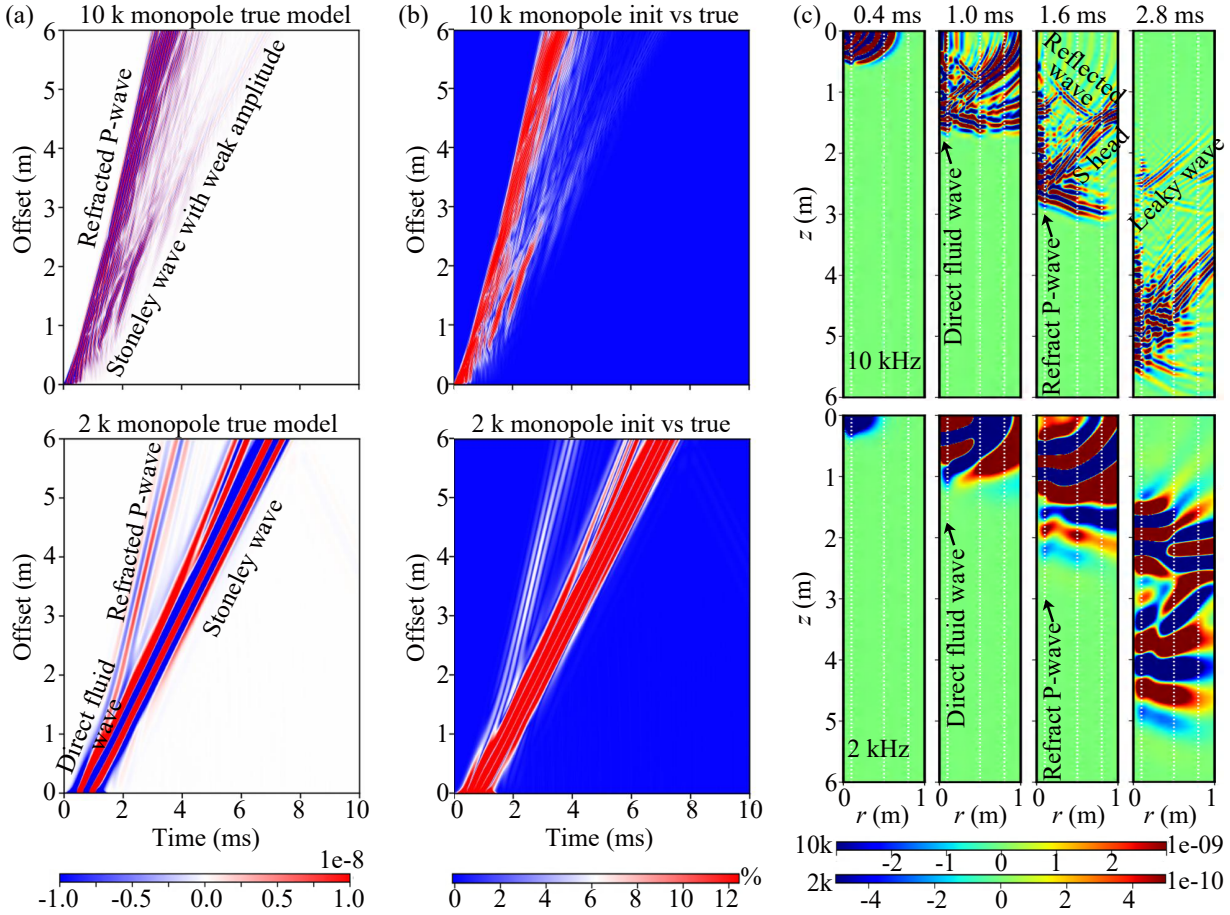

Fig. 3. Comparison of wavefields under 10 kHz and 2 kHz monopole excitation. (a) Time-domain waveforms; (b) Normalized absolute difference maps; and (c) Wavefield snapshots.

frequency monopole BFWI well-suited for recovering shear velocity in slow formations.

3.2 S-wave velocity profile inversion workflow

Based on the above observations, an S-wave velocity inversion workflow is formulated for slow formations. Assuming the availability of a P-wave velocity model, an initial S-wave model is generated by scaling the P-wave velocity using a constant velocity ratio. Low-frequency monopole BFWI is then performed to reconstruct the S-wave velocity distribution. This process is demonstrated in Fig. 4, where Fig. 4(a) illustrates the initial S-wave velocity model constructed by scaling the high-frequency P-wave inversion results using the V_P/V_S ratio. This approach provides a reasonable approximation of the S-wave structure, leveraging the typically better-resolved P-wave field as a foundation for subsequent inversion. The corresponding relative error in Fig. 4(b) reveals low errors near the borehole, with larger discrepancies at the outer radial boundaries. While this initial model may not capture fine-scale S-wave variations, it serves as a stable starting point for the low-frequency monopole BFWI process, especially in slow formations where S-wave information is limited. After 250 iterations, the inverted S-wave model closely matches the true model (Fig. 4(c)). The final relative error (Fig. 4(d)) is within 0.5% in most areas, except for slight deviations in the top and bottom corners due to limited illumination, validating the effectiveness of the proposed approach.

3.3 Ultraslow SEAM model

To evaluate the robustness of inversion, a special case is considered in which P- and S-wave structures are decoupled due to geological or fluid-related effects. In particular, ultraslow-velocity formations, common in shallow marine sediments or unconsolidated deposits, exhibit S-wave velocities as low as one-third that of the borehole fluid (Hornby and Murphy, 1987). To evaluate the robustness of our inversion workflow in this scenario, a subvolume near Well 2 was extracted from the SEAM open data model provided by the SEG Advanced Modeling Corporation. The targeted region within the SEAM model is presented (Fig. 5), including P-wave velocity (Fig. 5(a)), S-wave velocity (Fig. 5(b)), density (Fig. 5(c)), andthe V_P/V_S ratio (Fig. 5(d)). Notably, the S-wave velocity in this region is extremely low, reaching values as low as 700 m/s. Additionally, two distinct velocity anomaly zones are present, where the variations in P-wave and S-wave velocities are not correlated. This complexity provides an ideal scenario to evaluate the performance of the proposed inversion workflow. The test is designed to validate the robustness of

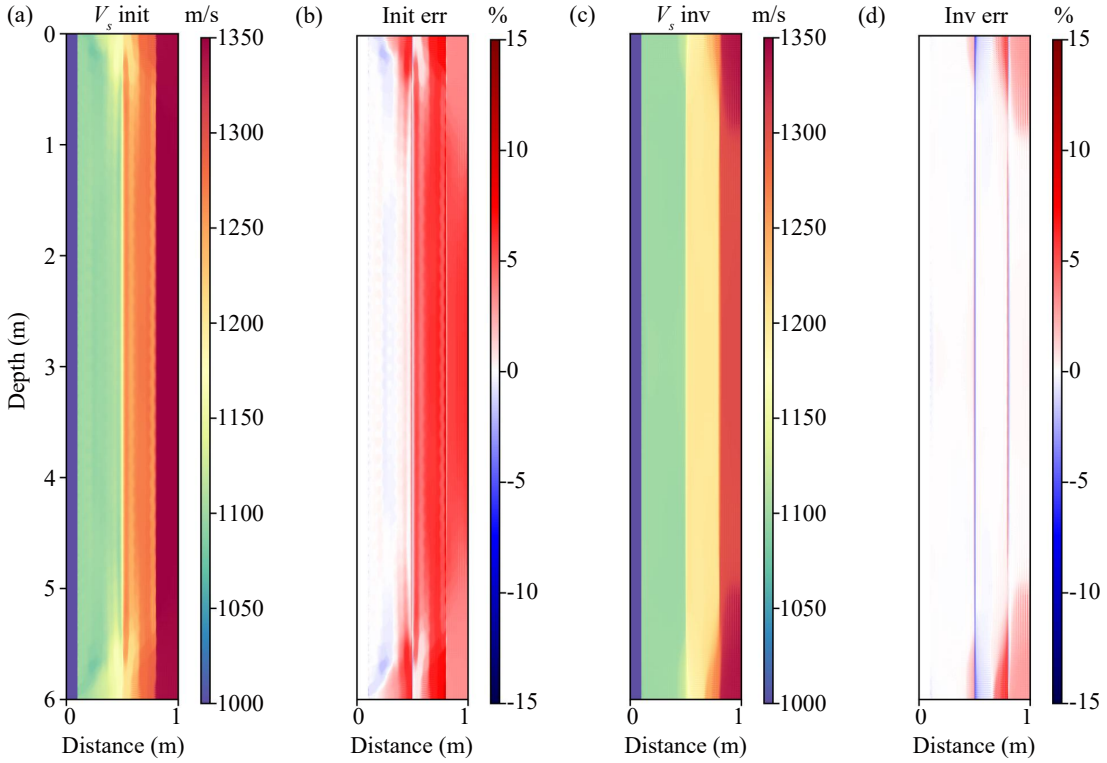

Fig. 4. Test of S-wave inversion workflow for slow formations using low-frequency monopole BFWI. (a) Initial model; (b) Initial error; (c) Inversion result after 250 iterations; and (d) Final error.

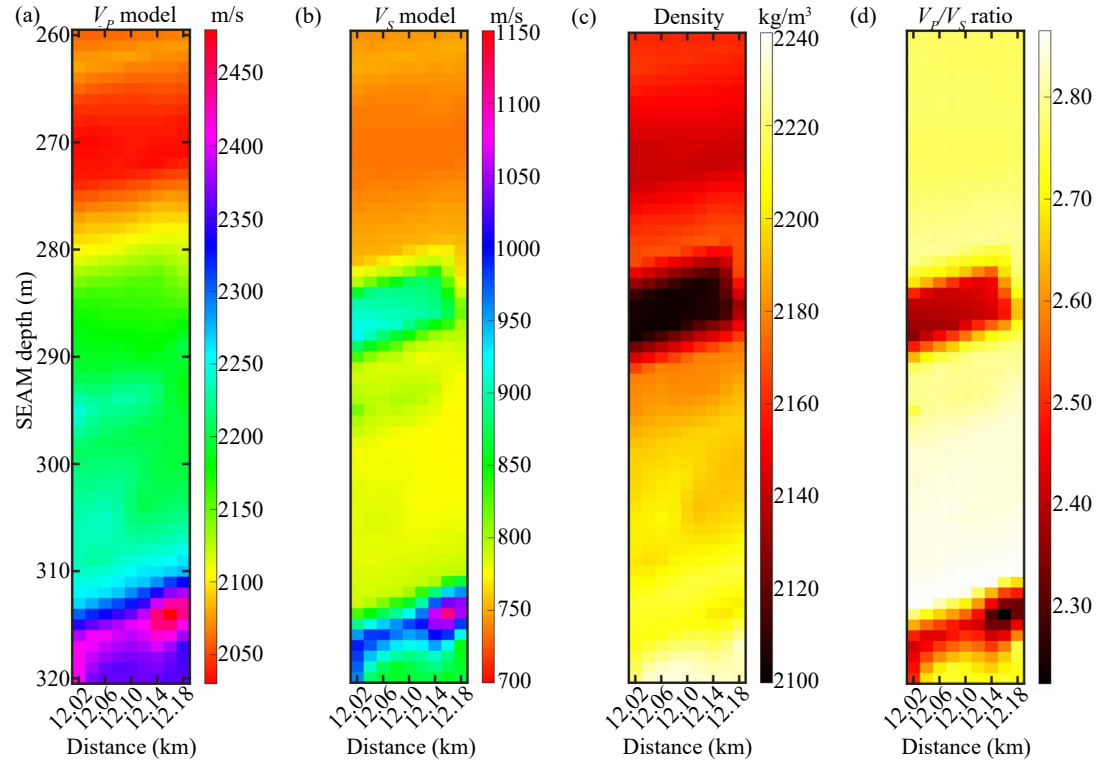

Fig. 5. SEAM-based test model extracted near Well 2, featuring S-wave anomalies in ultraslow formations. (a) V_P model; (b) V_S model; (c) Density model; and (d) V_P/V_S ratio.

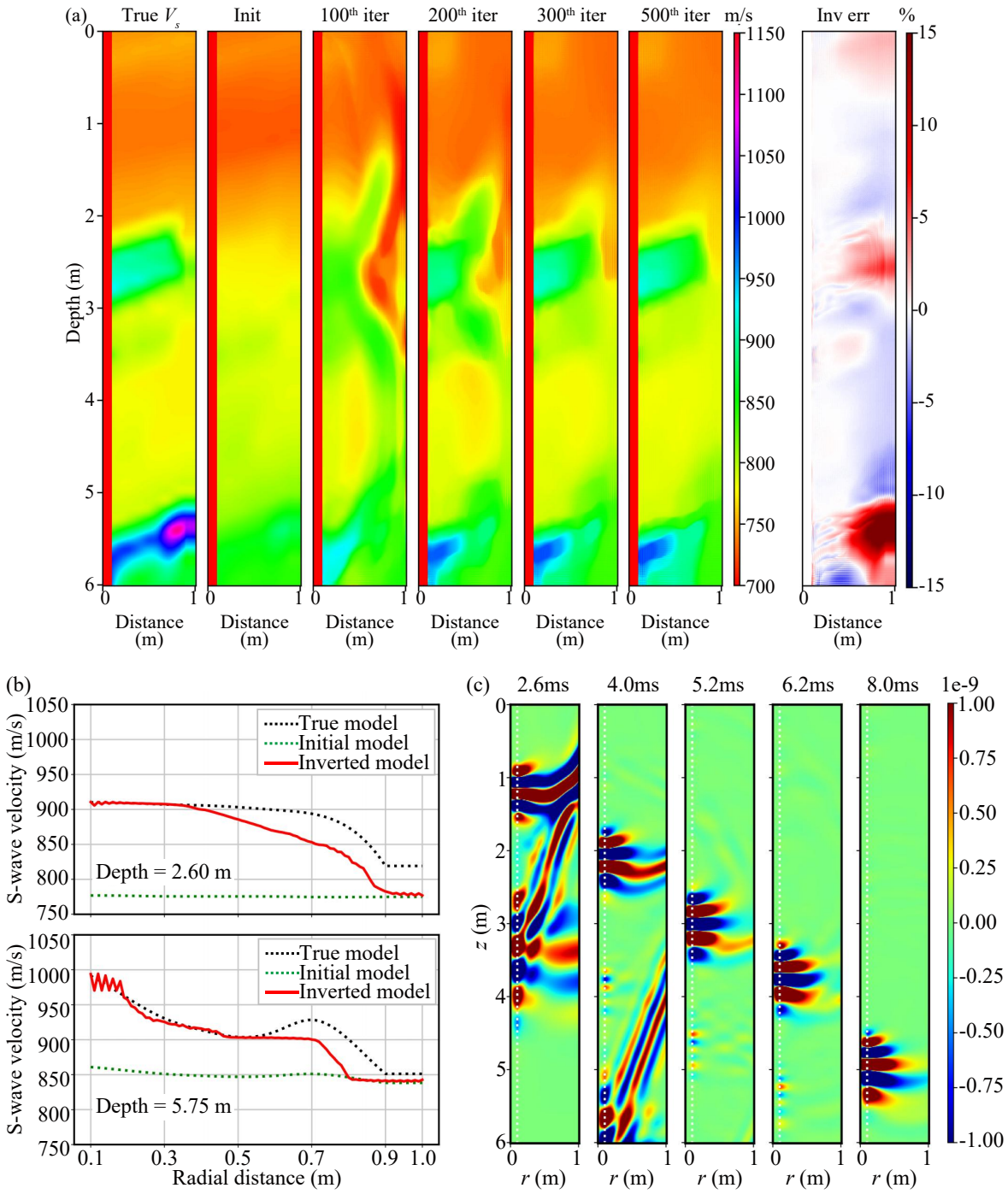

Fig. 6. Inversion results for the SEAM-based ultraslow model: (a) Evolution of S-wave velocity over iterations and final error; (b) Radial profiles at two S-wave anomaly depths; and (c) Wavefield snapshots showing Stoneley-wave effects.

our method under challenging velocity conditions. To adapt the model for borehole logging applications, geometric scaling was performed by reducing the depth dimension by a factor of 100 and the radial dimension by a factor of 200. In addition, grid refinement was applied to ensure numerical accuracy. The acquisition geometry was kept consistent with that used in previous tests. The inversion results are shown in Fig. 6.

Fig. 6(a) compares the true and initial S-wave velocity models. Although the initial model generated from the scaled P-wave structure captures the general trend, significant discrepancies remain in the two anomalous zones (2.0-3.0 m and 5.5-6.0 m). After 100 iterations at 2 kHz, the inversion begins to resolve the near-borehole anomalies (<0.3 m). With increasing iteration counts, the velocity artifacts are gradually suppressed. By iteration 500, the recovered model closely resembles the true S-wave distribution. The relative error analysis confirms that in the near-borehole region (<0.4 m), the error remains below 0.5%, though larger deviations persist

in deeper zones—particularly within the anomalous structures. Fig. 6(b) shows vertical velocity profiles at 2.60 m and 5.75 m depth. The initial models (green dashed lines) deviate significantly from the true structure (black dashed lines), while the inverted results (solid red lines) show excellent agreement near the borehole wall. The deeper anomaly at 5.75 m is better recovered due to its higher velocity and corresponding longer wavelength, which improves radial sensitivity. Despite some mismatch at larger radii, the overall velocity trend is accurately captured. Wavefield snapshots at selected time steps are shown in Fig. 6(c). Compared to the previous case, the Stoneley wavelength in this model is shorter, resulting in improved resolution near the borehole and superior inversion accuracy in the shallow zone. For ultralow-velocity formations, sufficient recording duration is essential to capture the full evolution of Stoneley waves and their contribution to S-wave imaging.

4. Conclusion

To address the challenge of S-wave velocity estimation in slow formations, a borehole full-waveform inversion approach has been developed by integrating automatic differentiation with a recurrent neural network representation of the elastic wave equation in cylindrical coordinates. This framework eliminates the need for traditional adjoint-state derivations, offering greater flexibility and scalability for multi-parameter inversion. This study establishes a fundamental relationship between monopole source frequency and the sensitivity of borehole wavefields to S-wave velocity in slow formations. Low-frequency monopole excitation enhances the generation and propagation of Stoneley waves, which remain highly sensitive to shear velocity even when critically refracted S-waves are absent. Based on this insight, a practical inversion workflow is introduced: high-frequency monopole data are first used to reconstruct the P-wave velocity model, which is then scaled by an empirical velocity ratio to generate the initial S-wave model. Subsequently, low-frequency inversion leveraging Stoneley-wave-dominated data is performed to recover the S-wave velocity distribution. Numerical experiments confirm the effectiveness of this strategy in both conventional slow formations and more complex geological settings, such as ultra-slow formations and models containing small-scale velocity anomalies. The proposed workflow provides a robust and generalizable solution for S-wave velocity estimation in environments where conventional methods fail, particularly in shallow unconsolidated sediments, near-seafloor soft muds, and borehole stability assessments where S-wave measurements are inherently difficult.

Acknowledgements

This work was supported by the Qingdao Natural Science Foundation (No. 24-4-4-zrjj-121-jch), United Fund of National Natural Science Foundation of China (No. U2344221), National Key R&D Program of China (Nos. 2022YFC2808302 and 2021YFC2801202) and the Young Talents Project Start-Up Foundation of Ocean University of China (No. 202212017). This research uses SEAM Open Data provided by the SEG Advanced Modeling Corporation under the Creative Commons Attribution 4.0 International License (CC BY 4.0). The authors gratefully acknowledge SEG for making the data publicly available (http://creativecommons.org/licenses/by/4.0/).

Conflict of interest

The authors declare no competing interest.

References

Berg, E. M., Lin, F. C., Schulte-Pelkum, V., et al. Shallow crustal shear velocity and V_P/V_S across Southern California: Joint inversion of short-period Rayleigh wave ellipticity, phase velocity, and teleseismic receiver functions. Geophysical Research Letters, 2021, 48(15): e2021GL092626.

Chen, D., Zhang, C., Guan, W., et al. Near-borehole formation acoustic logging imaging: A full waveform inversion algorithm in cylindrical coordinates. IEEE Transactions on Geoscience and Remote Sensing, 2023, 61: 4506414.

Du, B., Sun, J., Jia, A., et al. Physics-informed robust and implicit full waveform inversion without prior and low-frequency information. IEEE Transactions on Geoscience and Remote Sensing, 2024, 62: 5918712.

Ebrahimi, A., Izadpanahi, A., Ebrahimi, P., et al. Estimation of shear wave velocity in an Iranian oil reservoir using machine learning methods. Journal of Petroleum Science and Engineering, 2022, 209: 109841.

Engl, H. W., Hanke, M., Neubauer, A. Regularization of Inverse Problems. Dordrecht, The Netherlands, Kluwer Academic Publishers, 1996.

Fan, Y., Pang, H., Jin, Y., et al. Integration of image recognition and expert system for real-time wellbore stability analysis. Advances in Geo-Energy Research, 2025, 15(2): 158-171.

Fang, Z., Wang, H., Li, M., et al. A source independent TV-regularized full waveform inversion method for peripheral imaging around a borehole. IEEE Transactions on Geoscience and Remote Sensing, 2024, 62: 5916909.

Hornby, B. E. Tomographic reconstruction of near-borehole slowness using refracted borehole sonic arrivals. Geophysics, 1993, 58(12): 1726-1738.

Hornby, B. E., Murphy, W. F. V_p/V_s in unconsolidated oil sands: Shear from Stoneley. Geophysics, 1987, 52(4): 502-513.

Kurkjian, A. L., Chang, S.-K. Acoustic multipole sources in fluid-filled boreholes. Geophysics, 1986, 51(1): 148-163.

Li, J., He, X., Chen, H., et al. Inversion of radial shear velocity profile for acoustic logging using CNN-LSTM network. IEEE Transactions on Geoscience and Remote Sensing, 2024, 62: 5907610.

Li, J., Wan, J., Wang, T., et al. Leakage simulation and acoustic characteristics based on acoustic logging by

ultrasonic detection. Advances in Geo-Energy Research, 2022, 6(3): 181-191.

Li, J. C., He, X., Zhao, A. S., et al. Joint inversion of formation radial shear-velocity profiles by dipole acoustic logging while drilling. Geophysics, 2023, 88(4): D295-D305.

Mavko, G., Mukerji, T., Dvorkin, J. The Rock Physics Handbook. Cambridge, UK, Cambridge University Press, 2020.

Rajabi, M., Hazbeh, O., Davoodi, S., et al. Predicting shear wave velocity from conventional well logs with deep and hybrid machine learning algorithms. Journal of Petroleum Exploration and Production Technology, 2023, 13(1): 19-42.

Sinha, B., Vissapragada, B., Kisra, S., et al. Optimal well completions using radial profiling of formation shear slownesses. Paper SPE 95837 presented at SPE Annual Technical Conference and Exhibition, Dallas, Texas, 9-12 October, 2005.

Stevens, J. L., Day, S. M. Shear velocity logging in slow formations using the Stoneley wave. Geophysics, 1986, 51(1): 137-147.

Sun, J., Niu, Z., Innanen, K. A., et al. A theory-guided deep-learning formulation and optimization of seismic waveform inversion. Geophysics, 2020, 85(2): R87-R99.

Tang, H., Cheng, A. C. H., Li, Y. E., et al. Borehole acoustic full-waveform inversion. Geophysics, 2023, 88(4): D271-D293.

Tang, X. M., Cheng, C. H. A. Quantitative Borehole Acoustic Methods. Amsterdam, Netherlands, Elsevier, 2004.

Tang, X. M., Patterson, D. J. Mapping formation radial S-wave velocity variation by a constrained inversion of borehole flexural-wave dispersion data. Geophysics, 2010, 75(6): E183-E190.

Wang, B., Zhang, K. Direct inversion algorithm for shear velocity profiling in dipole acoustic borehole measurements. IEEE Geoscience and Remote Sensing Letters, 2018, 15(6): 828-832.

Wang, J., Cao, J., Yuan, S. Shear wave velocity prediction based on adaptive particle swarm optimization optimized recurrent neural network. Journal of Petroleum Science and Engineering, 2020, 194: 107466.

Wang, L., Ren, Z., Bao, Z. Full-waveform inversion of Rayleigh wave from high-speed-train seismic data for shallow-surface velocity building. Chinese Journal of Geophysics, 2025, 68(4): 1444-1456.

Wang, S., Jiang, Y., Song, P., et al. Memory optimization in RNN-based full waveform inversion using boundary saving wavefield reconstruction. IEEE Transactions on Geoscience and Remote Sensing, 2023a, 61: 5919212.

Wang, Y., Liu, Y., Zou, Z., et al. Recent advances in theory and technology of oil and gas geophysics. Advances in Geo-Energy Research, 2023b, 9(1): 1-4.

Xu, S. Integrated multipole acoustic modeling and processing in general stressed formations, Part 2: A well case study. Geoenergy Science and Engineering, 2024, 233: 212484.

Xu, S., Zou, Z. Perforation evaluation using multiscale traveltime tomography: Insights from borehole data. Geophysics, 2025, 90(3): A21-A25.

Xu, S., Zou, Z., Li, S. Offset-controlled localized velocity inversion in the tau-p domain using acoustic traveltimes: Modeling and application. IEEE Transactions on Geoscience and Remote Sensing, 2024, 62: 5936110.

Zeroug, S., Valero, H., Bose, S., et al. Monopole radial profiling of compressional slowness. SEG Technical Program Expanded Abstracts 2006, 2006, 354-358.

Zhang, C., Wang, H., Chen, D., et al. A full waveform inversion method for inverting S-wave velocity profiles of slow formations near borehole. Geoenergy Science and Engineering, 2025, 252: 213861.

Zhang, J., Lang, J., Standifird, W. Stress, porosity, and failure-dependent compressional and shear velocity ratio and its application to wellbore stability. Journal of Petroleum Science and Engineering, 2009, 69(3-4): 193-202.